Chemical Physics 136 (1989) 223–247
North-Holland, Amsterdam

NMR STUDY OF ENVIRONMENT MODULATED PROTON TAUTOMERISM IN CRYSTALLINE AND AMORPHOUS PHTHALOCYANINE

Bernd WEHRLE and Hans-Heinrich LIMBACH
Institut für Physikalische Chemie der Universität Freiburg i. Br., Albertstrasse 21, D-7800 Freiburg, FRG

Received 30 January 1989

Using high resolution ^{15}N and ^{13}C CPMAS NMR spectroscopy (CP – cross polarization, MAS – magic angle spinning) we have detected fast thermally activated proton transfer processes in solid ^{15}N enriched phthalocyanine (Pc). The synthesis of the latter is described. NMR experiments were performed on the crystalline α- and β-modifications, as well as on a novel amorphous modification (am-Pc). In order to extract thermodynamic and kinetic data from the NMR spectra an appropriate lineshape theory of bistable molecules in ordered and disordered matrices is developed. Bistable molecules are subject to exchange between at least two molecular states. The lineshape theory includes the possibility of site dependent perturbations of the rate and equilibrium constants of state exchange, as well as of exchange between different sites. For disordered environments bi-Gaussian distributions of the reaction enthalpies of the state exchange and of the enthalpies of activation are proposed. Different possibilities, including Marcus theory, of reducing this two-dimensional site distribution function to a one-dimensional distribution are discussed. The analysis of the NMR spectra gave the following results. Whereas the proton potential in α-Pc is quasisymmetric, the degeneracy of the tautomers in the β modification is lifted because of a subtle interplay between inter- and intramolecular interactions. The amorphous modification is characterized by a broad distribution of differently perturbed asymmetric double-minimum potentials, as expected for a disordered environment. Rotation of Pc in either of these modifications can be excluded. Proton transfer in the β phase is faster than in the α phase due to smaller energy of activation. This finding is interpreted with a different geometric arrangement of the inner nitrogen atoms in both phases. In addition, the proton transfer in the β phase is characterized by a smaller pre-exponential factor than in the α phase. This effect indicates substantial but different tunnel contributions to the reaction rates in both phases. The implications of the environment modulated proton transfer processes in Pc for the mechanism of hydrogen transfer reactions in liquids is discussed.

1. Introduction

To understand the mechanism of a chemical reaction it is necessary to know its energy surface [1,2]. For gas phase reactions this surface can be obtained from ab initio calculations of a single molecule or molecular complex. The situation in liquids and solids is, however, much more complicated because reacting species may experience different reaction energy surfaces depending on the molecular environment [3–6]. Information about such environmental effects is very difficult to obtain because liquid state rate constants generally represent averages over the different environments. The development of kinetic methods which are able to follow molecular dynamics in the regime of slow solvent relaxation is, therefore, of special importance.

In order to reach a timescale where solvent relaxation is slow, generally picosecond laser spectroscopy [4] has to be used when reactions in liquids are studied. This regime of slow molecular motions can, however, also be reached by dynamic NMR spectroscopy – which has proven to be a useful source of structural, thermodynamic and kinetic information [7–12] – when reactions in ordered crystals or disordered glasses are studied. Such studies have been made possible by the development of variable temperature high resolution solid state methods [13–16]. In these techniques spin 1/2 nuclei such as ^{13}C or ^{15}N atoms are monitored. Their dipolar couplings to protons are removed by proton decoupling and their chemical shift anisotropies are averaged by magic angle spinning (MAS); furthermore, sensitivity is enhanced by cross polarization (CP) from protons [13–15]. One main advantage of dynamic NMR spectroscopy over other kinetic methods is the possibility of studying sym-

metric exchange reactions where observed solid state perturbations of the reaction can be directly attributed to intermolecular interactions influencing the reaction energy surface [5,6]. Note that information about such solid state effects on chemical reactions is not only of the theoretical interest by may also have important technical applications [17].

Among the fastest reactions involving bond breaking and bond formation are proton, hydrogen atom, or hydride transfer reactions [2,18–26]. Generally, these reactions are associated with moving electric charges, i.e. they require major molecular solvent motions and are, therefore, often suppressed in the solid state. However, it has been shown that there is a category of fast hydrogen transfer reactions in and between polyatomic molecules [#1], where the reactants and products are neutral. As a rule, such processes require the transfer of more than one hydrogen atoms, e.g.

$$AH + BH \rightleftharpoons XH + YH\,.$$

Intra- and intermolecular reactions of this kind have been observed by NMR methods not only in the liquid [2,26,27–37] but also in the solid state [2,5,6,16,38–56]. Often these compounds are organic dyes, such as free base porphyrins [48–50,55,56], porphycene [50], phthalocyanine [16,49,54], tetraazaannulenes [5,6,52] and azophenine [37]. During the past decade, great progress has been made in the understanding of the mechanisms of these double-proton transfer reactions. For the elucidation of the reaction pathways the study of kinetic HH/HD/DD isotope effects as a function of temperature has been very useful [28,29,32,37,48,56]. Thus, not only tunneling contributions to the reaction rates have been verified but also information on the details of the proton motion has been obtained. Whereas in intermolecular double-proton transfer reactions both protons are in flight in the transition state [28,31], the intramolecular tautomerism of porphyrins and related compounds proceeds along symmetric triple minimum potentials via two consecutive single-proton transfer steps [29,36,37,56]. In two cases the intermediates have been directly observed by NMR spectroscopy [50,51]. An explanation of the different behavior of the inter–intramolecular proton transfer systems has been given recently [28]. Calculated energy surfaces using semi-empirical and ab initio methods support the stepwise tunneling mechanism in porphyrins and azophenine [57–62]. Note that organic dyes such as Pc are also subject to phototautomerism [63–70] which can even occur at cryogenic temperatures, as detected by hole burning techniques. Such systems have, therefore, been proposed as components in future optical information storage devices [17,65,69].

Therefore, we study in this paper the problem of environmentally modulated proton tautomerism of phthalocyanine (Pc) shown in fig. 1. The localisation and transfer of the protons in the solid phases of these dyes has been an old problem of solid state crystal structure analysis [71–83] and was the subject of controversial discussions over the past decades. Whereas the tautomerism of porphyrins was studied very early using liquid state NMR methods [27,29], the insolubility of Pc in organic liquids has been a major reason why little is known about the location and the dynamics of the inner protons in this compound. For a long time, this problem has been subject of much speculation [78–81], especially in view of the fact that Pc can exist in several crystal modifications [82–87]. Most research has been reported on the α and β phases. Although Robertson [78] had

[#1] Since neither protons nor other ions are educts or products in these reactions, strictly speaking only the term hydrogen transfer which includes the possibility of the transfer of protons, hydrogen atoms, or hydride ions would be correct; however, since protons are, generally, transfered in hydrogen bonded systems we will use here the term proton transfer.

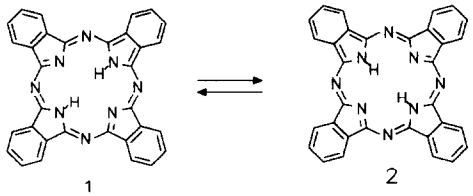

1 2

Fig. 1. The tautomerism of phthalocyanine (Pc).

already determined the crystal structure of the β phase by X-ray analysis in 1936, the problem of tautomerism remained. A neutron scattering study on this modification found the hydrogen atoms equally distributed on the four inner nitrogen atoms [80]. For the α modification no crystal structure analysis has yet been performed. The first indications for a dynamic proton transfer in Pc came from ^{15}N CPMAS NMR spectroscopy of β-Pc [16,49] which were subsequently supported by ^{13}C NMR experiments on α-Pc [54]. These measurements showed differences in the behavior of both phases which have not yet been correlated to the molecular structure. One goal of this study is, therefore, to elucidate the different proton transfer characteristics in both phases. In addition, we have found also a novel amorphous modification (am-Pc) where we have studied the question of how the tautomerism is influenced when the ordered lattice breaks down. Since nitrogen atoms are part of the NH...N proton transfer units we preferentially use ^{15}N CPMAS NMR spectroscopy of ^{15}N enriched Pc [16,49], although ^{13}C experiments were also carried out which provide interesting additional structural information. Unfortunately, because of the low natural abundance and the absolute low sensitivity of the ^{15}N nuclei it is necessary to artifically enrich the samples with that isotope in order to record exchange broadened ^{15}N CPMAS NMR spectra.

This paper is organized as follows. After an experimental section, section 2, where the synthesis of Pc-$^{15}N_8$ and its precursor *o*-phthalodinitrile-$^{15}N_2$ is described, we present the NMR lineshape theory used to analyze the experimental Pc spectra in the ordered crystalline and amorphous modifications. This theory, which takes into account a distribution of differently shaped double minimum potentials of the reaction is an extension of a previously published theory of CPMAS NMR lineshapes of bistable molecules in disordered matter. The case of a superposition of different chemical rate processes in different reaction sites is also incorporated. Previously, only equilibrium effects and site exchange were taken into account [5,6]. After the theoretical section, section 3, we describe the ^{15}N as well as some ^{13}C CPMAS NMR experiments performed on Pc. The different kinetic and thermodynamic properties found are then discussed against the background of the known solid state structure of phthalocyanine.

2. Experimental

2.1. Synthesis of ^{15}N-enriched phthalocyanine

Since ^{15}N labeled phthalocyanine has, to our knowledge, not yet been prepared, we describe here all necessary procedures for its synthesis, including the synthesis of the ^{15}N labeled precursor *o*-phthalodinitrile. The latter is, generally, obtained from phthalic anhydride and ammonia via phthalimide and phthalamide, followed by a dehydration step. From the standpoint of isotopic enrichment this route is inefficient because it requires isolation and purification of the intermediates. Therefore, a low cost method for the preparation of ^{15}N enriched phthalodinitrile had to be developed which uses a minimum input of $^{15}NH_4Cl$. For this purpose we have modified an industrial synthesis of phthalodinitrile from phthalic anhydride and gaseous ammonia without isolation of the intermediates [88] (fig. 2) for use on a laboratory scale. This reaction is also suitable for the synthesis of substituted ^{15}N enriched phthalodinitriles, e.g. 4-*t*-butylphthlalocyanine. Thus, we were able to prepare soluble ^{15}N-labeled phthalocyanines as well.

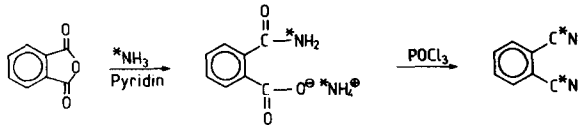

Fig. 2. Synthesis of ^{15}N enriched phthalocyanine.

2.1.1. Synthesis of o-phthaloditrile-$^{15}N_2$

1.48 g (10 mmol) of purified phthalic anhydride was dissolved in 7.5 ml pyridine (dried over KOH). The solution was cooled to −40°C using a methanol/CO_2 mixture. Gaseous $^{15}NH_3$ was developed from 1.2 g 95% ^{15}N labeled ammonium chloride in an apparatus similar to the one described by Clusius and Effenberger [89] and condensed into a vessel cooled to liquid nitrogen temperature. In the next step it was condensed in small amounts into the reaction flask, still kept at −40°C. After complete addition the temperature was adjusted to 75°C and excess ammonia was removed under continuous stirring by a slow passage of gaseous nitrogen. The precipitate was dehydrated by adding freshly distilled $POCl_3$ in small portions to the reaction mixture. During this highly exothermic reaction step the temperature had to be kept below 80°C in order to avoid the formation of by-products. The limpid solution was poured into a strongly stirred ice/water mixture (5 g/10 g) and neutralized with 5*n* H_2SO_4. The precipitate was filtered and washed with 15 ml H_2O. In order to remove traces of acid the raw product was suspended in 5.5 g 2% KOH and stirred for 10 min. After filtration and drying at 80°C 450 mg *o*-phthalodinitrile-$^{15}N_2$ was obtained (34.5% yield, Fp. 138–139°C). The product was further characterized by IR spectroscopy.

2.1.2. Synthesis of phthalocyanine-$^{15}N_8$

$^{15}N_8$-phthalocyanine was synthesized according to the procedure of Linstead and Lowe [90] given for the unlabeled material. For this purpose 250 mg *o*-phthalonitrile-$^{15}N_2$ were added to a solution of sodium (45 mg) in amylalcohol (0.5 ml). The reaction mixture was boiled for one hour, cooled to room temperature and diluted with ethanol. After filtration the raw product was boiled several times with ethanol in order to remove a brown by-product. Thus, 92 mg of chemically pure ^{15}N-labeled phthalocyanine was obtained. In the mass spectrum several molecule ion peaks at 521 (weak), 522 (strong), 523 (weak) and 524 (very weak) were found. Since the ^{15}N content of the ammonium chloride was of the order 95% we attribute the strongest peak at 522 to phthalocyanine-$^{15}N_8$. In the elemental analysis it was found that C = 72.68, N = 21.22 and H = 3.56, which compares well with the calculated values C = 73.56, N = 22.99, and H = 3.45.

2.1.3. Synthesis of different phthalocyanine modifications

The α modification of ^{15}N labeled Pc was obtained according to the literature [83] by recrystallization of the crude product from concentrated sulfuric acid. The conversion into the β modification was achieved by annealing the material for 3 days at 300°C and 1 atm [86,87]. The two modifications were distinguished and identified by their X-ray diffraction powders and by their IR spectra [84–87].

The novel amorphous modification (am-Pc) was obtained by attempting to sublime the β modification in vacuo at 300°C. In the mass spectrum of the residue no Pc-molecule ion peak could be detected. A strong peak at 44 arising from CO_2 indicates that the material decomposes under the measuring conditions of mass spectroscopy. There are also indications in the mass spectra that during the heating process some phthalic anhydride might be formed. By contrast, the IR spectra were found to be similar to the crystalline modifications. Nevertheless, the C–H deformation stretching band is broad and featureless. The elemental analysis gave C = 65.63, N = 18.63 and H = 2.76 as compared to the calculated values C = 73.56, N = 22.99 and H = 3.45. As shown later, the solid state ^{15}N CPMAS NMR spectra did not show ^{15}N containing impurities.

2.2. NMR measurements

All NMR experiments were performed on a Bruker CXP 100 NMR spectrometer working at 90.02 MHz for ^1H, at 9.12 MHz for ^{15}N, and at 22.63 MHz for ^{13}C. The spectrometer was equipped with a 2.1 T wide-bore Bruker cryomagnet. The CPMAS NMR experiments were performed using a Doty MAS probe [91]. In the low-temperature experiments the driving nitrogen gas was cooled with liquid nitrogen with a home-built heat-exchanger described elsewhere [16]. The sample temperature was monitored with a Pt resistance thermometer placed close to the sample.

3. Theoretical

In this section we present a high-resolution NMR lineshape theory of spin 1/2 nuclei in bistable molecules embedded in solids. These molecules interconvert in the gas phase between two isomeric states 1 and 2. As has been shown previously [5,6], matrix effects in disordered matrices like glasses or other amorphous solids can be modeled in terms of different environments or "sites" in which the bistable molecules experience different equilibrium constants of isomerism. In our previous studies [5,6] we calculated NMR lineshapes for the case of fast isomerism as a function of the parameters of an appropriate site distribution function. The effects of exchange between the different sites were also included in the theory. However, in the absence of an experimental example sites with different rate constants of isomerism were not yet taken into account. Since this case is realized for amorphous phthalocyanine it will be included here.

3.1. General NMR lineshape theory of chemical exchange

The theory of exchange broadened pulse FT NMR spectra has been described previously [8–12]. The free induction decay signal measured in the NMR experiment depends on the off-diagonal elements of the density matrix ρ of the spin ensemble studied. In Liouville space the time dependence of these elements is governed by the master equation

$$d\rho/dt = \mathcal{M}\rho ,$$

$$\mathcal{M} = -2\pi i(\mathcal{L} - \nu\epsilon) + \mathcal{R} + \Xi . \tag{1}$$

In eq. (1) ϵ is the unit matrix, ν the frequency in Hz, $\mathcal{L}$ the Liouville operator, $\mathcal{R}$ the transverse part of the Redfield relaxation matrix, and Ξ the operator describing the chemical exchange. Let k and l be indices characterizing the rows and the comlumns of the matrix $\mathcal{M}$. The element of $\mathcal{M}$ are then written as $\mathcal{M}_{kl}$. k respectively l correspond to transition or quantum coherences between the spin states α and β respectively α' and β'. The elements of $\mathcal{L}$ are given by

$$\mathcal{L}_{kl} = \mathcal{L}_{\alpha\beta\alpha'\beta'} = \mathcal{H}_{\alpha\alpha'}\delta_{\beta\beta'} - \mathcal{H}_{\beta\beta'}\delta_{\alpha\alpha'} . \tag{2}$$

δ is the Kronecker symbol and $\mathcal{H}$ the Hamilton operator, which can be written as the sum

$$\mathcal{H} = \sum_{\kappa} \mathcal{H}_{\kappa} , \tag{3}$$

$\mathcal{H}_{\kappa}$ is the Hamiltonian of the κth environment, isomer, state, etc. which participates in the exchange. $\mathcal{H}_{\kappa}$ acts only on the spin functions in κ. Thus, each diagonal element of $\mathcal{M}$ can be associated with a certain molecular state κ. In the absence of spin–spin coupling the Redfield relaxation operator $\mathcal{R}$ is diagonal. Generally, one includes artificial and apparative line broadening in the diagonal elements, given by $-\pi W_0$, where W_0 is the effective linewidth in Hz in the absence of exchange. The exchange operator Ξ depends on the rate constants of the exchange and the particular exchange problem. The dimension of $\mathcal{M}$ is given by the number of NMR transitions. Each transition n is characterized by the position Λ_n^{im} and the width Λ_n^{re}, where $\Lambda_n = \Lambda_n^{\mathrm{re}} + i\Lambda_n^{\mathrm{im}}$ corresponds to the eigenvalues of the matrix $\mathcal{M}$, calculated by diagonalization of $\mathcal{M}$ according to the transformation [10]

$$\Lambda = C^{\mathrm{l}}\mathcal{M}C^{\mathrm{r}} . \tag{4}$$

Each transition is also characterized by a complex intensity

$$Q_n = Q_n^{\mathrm{r}} + iQ_n^{\mathrm{i}} = \left(\sum_k I_k^{-} C_{kn}^{\mathrm{r}}\right)\left(\sum_l \rho_l(0) C_{nl}^{\mathrm{l}}\right), \tag{5}$$

where I_k^- are the elements of the lowering operator, which are unity for one-spin systems, and $\rho_k(0)$ the elements of the density matrix at $t=0$ given by

$$\rho_k(0)=f_k P_k I_k^- . \tag{6}$$

Since the elements I_k^- and $\rho_k(0)$ are associated with a given molecular state κ the quantities P_k correspond to the molecule fractions P_κ of this state. f_k describes deviations of the elements $\rho_k(0)$ from $P_k I_k^-$. f_k depends on the pulse sequence used and the type of spin system studied. For simple nonselective 90° pulses applied on one-spin systems all $f_k=1$. In CPMAS experiments $f_k \neq 1$ because of the different polarization dynamics of inequivalent spins. In the absence of spin–spin coupling, i.e. the case where each supermolecular state κ gives rise to only one diagonal element in $\mathcal{M}$, i.e. one spectral transition k (see previous section), k and κ are identical. Then, the elements of the density matrix vector, $\rho_k(0)=\rho_\kappa(0)=f_\kappa P_\kappa$, according to eq. (6). Finally, the lineshape function is conveniently written in the form

$$Y(\nu) \approx \sum_n \{[Q_n^{re} \Lambda_n^{re} - Q_n^{im}(\Lambda_n^{im} - 2\pi\nu)]/[(\Lambda_n^{re})^2 + (\Lambda_n^{im} - 2\pi\nu)^2]\} . \tag{7}$$

In actual calculations it is only necessary to set up the matrix $\mathcal{M}$ and the vector $\rho(0)$. If the Hamiltonian only consists of terms arising from isotropic chemicals shifts, and if each environment κ contains only one nucleus with the chemical shift ν_κ, one observes in the slow exchange range singlets, one for each environment, with an intensity corresponding to the population of the environment, if all $f_\kappa=1$. As the exchange becomes faster the lines broaden and coalesce. In the fast range only an averaged line survives whose position is given by

$$\nu = \sum_\kappa P_\kappa \nu_\kappa . \tag{8}$$

3.2. Lineshapes theory of state and site exchange in a finite number of sites

The isomerism of a bistable molecule between two molecular states can be expressed by the equation

$$1 \rightleftharpoons 2 \tag{9}$$

when the reaction takes place in the gas phase or in the ordered solid state. However, when the molecules are embedded in disordered solids [5,6] a multitude of different reaction sites m has to be taken into account

$$1m \rightleftharpoons 2m, \quad m = 1, 2, ..., l , \tag{10}$$

where the molecules experience different equilibrium constants

$$K_{1m2m} = P_{2m}/P_{1m} = k_{1m2m}/k_{2m1m} . \tag{11}$$

In eq. (11) $P_\kappa = P_{im}$ is the population of state i = 1, 2 in site m; $\kappa = im$ characterizes the "supermolecular state". k_{1m2m} and k_{2m1m} are the forward and the backward rate constants in site m. We now extend our previous [5,6] site definition and define a site m as the ensemble of all bistable molecules characterized by the same forward and backward rate constants of the isomerism. The mole fraction of this site is then given by

$$P(m) = P_{1m} + P_{2m} . \tag{12}$$

The individual populations P_{im} can easily be calculated from eqs. (11) and (12):

$$P_{1m} = \frac{1}{1+K_{1m2m}} P(m), \quad P_{2m} = \frac{K_{1m2m}}{1+K_{1m2m}} P(m) . \tag{13}$$

The exchange operator Ξ connects two individual supermolecular state $\kappa = im$ and $\kappa' = jn$. Taking into consideration the principle of detailed balance, the elements of the exchange operator Ξ are given by [10]

$$\Xi_{\kappa\kappa'} = -\delta_{\kappa\kappa'} \sum_{\kappa'' \neq \kappa} k_{\kappa\kappa''} + (1-\delta_{\kappa\kappa'}) k_{\kappa\kappa'} \,. \tag{14}$$

$\delta_{\kappa\kappa'}$ is the Kronecker symbol and $k_{\kappa\kappa'} = k_{imjn}$ the pseudo-first-order rate of exchange between the states $\kappa = im$ and $\kappa' = jn$, i, j = 1, 2. The quantity k_{imjm} then corresponds to the state exchange in site m, the quantity k_{imin} to the exchange between the sites m and n, the molecular state i staying the same. If state exchange and site exchange occur statistically independent from each other it is a good approximation to set

$$k_{1m1n} = k_{2m2n} = k_{mn}, \quad \text{and} \quad k_{imjn} = 0 \quad \text{for } m \neq n \text{ and } i \neq j \,. \tag{15}$$

The exchange operator may then the rewritten in the form

$$\Xi_{\kappa\kappa'} = \Xi_{imjn} = -\delta_{ij} \sum_{k \neq i} \delta_{mn} k_{imkn} + (1-\delta_{ij}) \delta_{mn} k_{imjn} - \delta_{mn} \sum_{r \neq m} \delta_{ij} k_{imjr} + (1-\delta_{mn}) \delta_{ij} k_{imjn}; \quad i, j, k = 1, 2 \,. \tag{16}$$

The first two terms describe the state exchange in *one* site, the last two exchange between different sites m. The expression

$$\tau_m^{-1} = \sum_{r \neq m} \delta_{ij} k_{imjr} \tag{17}$$

is the inverse lifetime of site m. Site exchange in the limit of fast state exchange has been treated in detail in a previous paper [6]. In this article we focus on infinite long site lifetime τ_m. The exchange operator then reduces to

$$\Xi_{\kappa\kappa'} = \Xi_{imjn} = -\delta_{ij} \sum_{k \neq i} \delta_{mn} k_{imkn} + (1-\delta_{ij}) \delta_{mn} k_{imjn}; \quad i, j, k = 1, 2 \,. \tag{18}$$

The further treatment now depends on whether one has to consider only a small number of sites as in ordered crystals or a larger number as in disordered solids. In the latter case it will be necessary to introduce appropriate site distribution functions as shown below.

3.3. Calculated lineshapes for molecular isomerism in two sites

Let us consider now the simplest reaction network shown in scheme 1 where a bistable molecule exchanging between two states 1 and 2 can exist in two sites *1* and *2*. Let each site m and state i contain only one spin, whose Larmor frequency is given by the isotropic chemical shift ν_{im}. The intrinsic linewidth in the absence of exchange is then W_{0im}. From eqs. (1) and (16) it follows that

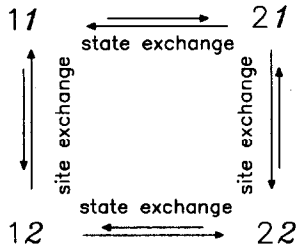

Scheme 1.

$$\mathcal{M}=\begin{array}{c} \\ 11 \\ 21 \\ 12 \\ 22 \end{array}\begin{array}{c} \begin{array}{cccc} 11 & 21 & 12 & 22 \end{array} \\ \begin{pmatrix} -k_{1121}-k_{1112}-\pi W_{011}-2\pi i\nu_{11} & k_{2111} & k_{1211} & \\ k_{1121} & -k_{2111}-k_{2122}-\pi W_{021}-2\pi i\nu_{21} & & k_{2221} \\ k_{1112} & & -k_{1222}-k_{1211}-\pi W_{012}-2\pi i\nu_{12} & k_{2212} \\ & k_{2122} & k_{1222} & -k_{2212}-k_{2221}-\pi W_{022}-2\pi i\nu_{22} \end{pmatrix} \end{array}, \tag{19}$$

with $\rho_{im}(0)=P_{im}$. The NMR lineshape is then easily calculated according to the procedures outlined in section 3.2. Generally, the parameters in eq. (19) are determined by fitting the calculated spectra to the experimental spectra.

In order to demonstrate typical spectral patterns it is interesting to discuss some special cases included in eq. (19), relevant to the kind of exchange problems studied experimentally in this paper. Thus, let the following relations hold:

$$k_{1121}=k_{2212},\quad k_{2111}=k_{1222}, \tag{20}$$

i.e.

$$K_{1121}=K_{1222}^{-1}. \tag{21}$$

Furthermore, let

$$k_{1112}=k_{2221},\quad k_{1211}=k_{2122}, \tag{22}$$

hold, from which it follows that

$$P_{11}=P_{22}\neq P_{21}=P_{12}. \tag{23}$$

In the following, we call two sites for which eqs. (20)–(23) hold also "twin" sites. Let us further set

$$\nu_{11}\approx\nu_{12}\equiv\nu_1,\quad \nu_{21}\approx\nu_{22}\equiv\nu_2,\quad \text{with } \Delta\nu=\nu_1-\nu_2. \tag{24}$$

This choice of parameters is typical for symmetric proton transfer systems of the type

$$^{15}N_AH...^{15}N_X \rightleftharpoons {}^{15}N_A...^{15}HN_X, \tag{25}$$

where the molecular structure is such that the nitrogen atoms A and X are equivalent in the absence of intermolecular interactions, i.e. where the two tautomers in eq. (25) are degenerate. By contrast, in the presence of intermolecular interactions in an ordered crystal, generally, solid state perturbations are observed which lift the degeneracy of the two tautomers [48–52]. Thus, there are two equivalent ways of incorporating the molecule in the solid, in other words, the molecule has access to two sites. The resulting reaction network is shown in scheme 2. In site *1* spin A is placed on the "left" and X on the "right" side of the unit cell. Since the two tautomers 1*1* and 2*1* are no more degenerate, the proton is preferentially located on nucleus A. By contrast, in site *2* nucleus X is placed on the left and A on the right side. Thus, the proton is located preferentially on nucleus X. Both sites *1* and *2* have the same probability because of eq. (23).

Because of the symmetry relations (20)–(24) between the two nuclei, the contributions of nuclei A and X to the NMR lineshapes are identical in the absence of spin–spin interactions and we can use eq. (19) in order to calculate the NMR lineshapes shown in figs. 3 and 4. In a first series of calculated spectra (fig. 3, lower part) we set the site exchange constant $k_{imn}=0$ and varied only the state exchange rate constants. The equilibrium constant $K_{1121}=K_{2212}^{-1}$ was set to a value of 0.33 in all spectra. In the slow state exchange region two sharp lines are

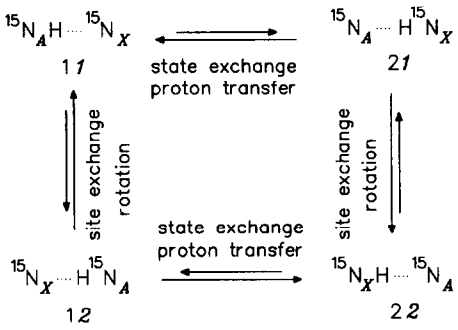

Scheme 2.

observed. When the state interconversion rate constant $k_{1\,21}$ is increased, the two lines broaden and sharpen again. In the fast exchange region two sharp lines are expected whose frequencies are given by

$$\nu_1 = P_{11}\nu_{11} + (1-P_{11})\nu_{21} = (\nu_1 + K_{1\,21}\nu_2)/(1+K_{1\,21}) = (\nu_1 + K_{1\,22}^{-1}\nu_2)/(1+K_{1\,22}^{-1}) , \tag{26}$$

$$\nu_2 = P_{12}\nu_{12} + (1-P_{12})\nu_{22} = (\nu_1 + K_{1\,22}\nu_2)/(1+K_{1\,22}) = (\nu_1 + K_{1\,21}^{-1})/(1+K_{1\,21}^{-1}) . \tag{27}$$

For the reduced splitting between the two lines it follows that

$$\delta\nu = \nu_2 - \nu_1 = \Delta\nu(1-K_{1\,21})/(1+K_{1\,21}) . \tag{28}$$

In order to calculate the equilibrium constant $K_{1\,21} = K_{1\,22}^{-1}$ from the reduced splitting $\delta\nu$ it is necessary to know the intrinsic chemical shift difference $\Delta\nu = \nu_1 - \nu_2$.

In the upper half of fig. 3 the site exchange rate constants $k_{i\,min}$ are increased. Now, the two averaged lines broaden and coalesce into one sharp line. It follows, as stated previously [5,6], that the observation of a reduced

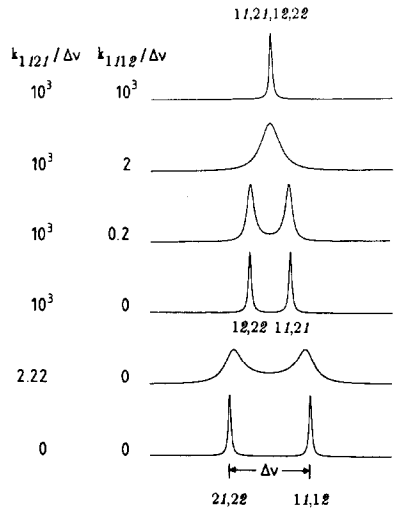

Fig. 3. Calculated spectra for a bistable molecule located in an asymmetric site, subject to exchange between two molecular states and two molecular sites. The rate constant $k_{1\,21}$ describes the state exchange, the $k_{1\,12}$ describes the site exchange, i.e. rotation of the molecule. The equilibrium constant $K_{1\,21} = K_{1\,12}$ was set to a value of 0.33 in all spectra.

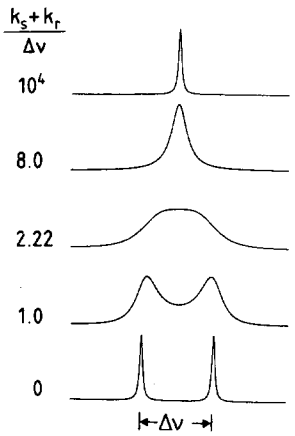

Fig. 4. Calculated spectra of bistable molecule located in a symmetric site where $K_{1\,21} = K_{1\,22} = 1$. k_s and k_r are the state and site exchange rate; not that only the sum can be detected.

doublet indicates absence of A–X interchange via molecular rotations in the case of symmetric bistable compounds.

We now come to the special case with equal populations of states 1 and 2, i.e. where $K_{1\,2\,1}=K_{1\,2\,2}=1$. In this case

$$k_{1\,2\,1}=k_{2\,1\,1}=k_{\mathrm{s}},\quad k_{1\,1\,2}=k_{\mathrm{r}}\,. \tag{29}$$

One can then easily show that the lineshape depends on the sum $k=k_{\mathrm{s}}+k_{\mathrm{r}}$ only. Then, the familiar symmetric line shapes shown in fig. 4 result with two lines in the slow and one averaged center line in the fast state/site exchange region.

3.4. The case of more than two superposed sites with different equilibrium constants

In this section we take a multitude of different sites m into account. Among different possibilities of site selection we chose the following. We arbitrarily define a site m as the ensemble of nuclear spins experiencing the equilibrium constant

$$K_{1m2m}=(m-1)/(l-m)\,. \tag{30}$$

l is the maximum number of sites taken into account. Note that the equilibrium constants for site m and for $m'=l-m+1$ are related according to

$$K_{1m'2m'}=K_{1m2m}^{-1}\,. \tag{31}$$

Therefore, m and m' are twin sites. In symmetrical molecules for which eq. (23) is valid, the probabilities of sites m and m' are equal:

$$P(m)=P(m')\,. \tag{32}$$

Let us now assume again that

$$\nu_{1m}\approx\nu_{1n}=\nu_1,\quad \nu_{2m}\approx\nu_{2n}=\nu_2=\nu_1+\Delta\nu\,. \tag{33}$$

Extending eqs. (26) and (27) we obtain for the position of the averaged lines in the fast state exchange range

$$\nu_m=\nu_1+(m-1)(\nu_2-\nu_1)/(l-1);\quad m=1,\ldots,l\,. \tag{34}$$

We now have to introduce an appropriate site distribution function, either a discontinuous function $P(K_{1m2m})$, or a continuous function $P(K_{12})$. In previous studies we found that a bi-Gaussian distribution of free energies of state exchange ΔG_{12} is appropriate to describe bistable molecules in the disordered solid state [5,6]. ΔG_{12} is related to the equilibrium constant of state exchange by the van 't Hoff equation

$$K_{12}=\exp(-\Delta G_{12}/RT)\,. \tag{35}$$

Here R is the gas constant and T temperature in kelvin. The distribution function reads [5,6]

$$P(\Delta G_{12})=-\frac{1}{N}\frac{\mathrm{d}N}{\mathrm{d}\Delta G_{12}}=\frac{1}{2}\left(\frac{\gamma}{\pi}\right)^{1/2}\{\exp[-\gamma(\Delta G_{12}-\overline{\Delta G}_{12}-\Delta G_{12}^{\mathrm{m}})^2]$$

$$+\exp[-\gamma(\Delta G_{12}-\overline{\Delta G}_{12}+\Delta G_{12}^{\mathrm{m}})^2]\}\,,\quad \gamma=1/2\sigma^2\,. \tag{36}$$

This function is characterized by two maxima, one at $\overline{\Delta G}_{12}+\Delta G_{12}^{\mathrm{m}}$ and the other at $\overline{\Delta G}_{12}-\Delta G_{12}^{\mathrm{m}}$. $\overline{\Delta G}_{12}$ is the mean free reaction enthalpy of the isomerism. The expression $(\sigma^2+\Delta G_{12}^{\mathrm{m}})^{1/2}$ characterizes the width of the distribution [6]. By combining eqs. (30) and (34) it follows that

$$P(m)=\frac{1}{N}\frac{\mathrm{d}N}{\mathrm{d}m}=\frac{1}{N}\frac{\mathrm{d}N}{\mathrm{d}\Delta G_{12}}\frac{\mathrm{d}\Delta G_{12}}{\mathrm{d}K_{12}}\frac{\mathrm{d}K_{12}}{\mathrm{d}\nu}\frac{\mathrm{d}\nu}{\mathrm{d}m}=\left(\frac{\gamma}{\pi}\right)^{1/2}\frac{RT}{2}\frac{l-1}{(m-l)(m-1)}$$
$$\times\left\{\exp\left\{-\gamma\left[-RT\ln\left(\frac{m-1}{l-m}\right)-\overline{\Delta G}_{12}-\Delta G_{12}^{\mathrm{m}}\right]^2\right\}+\exp\left\{-\gamma\left[-RT\ln\left(\frac{m-1}{l-m}\right)-\overline{\Delta G}_{12}+\Delta G_{12}^{\mathrm{m}}\right]^2\right\}\right\}. \tag{37}$$

In actual calculation one has to vary σ, $\overline{\Delta G}_{12}$ and $\Delta G_{12}^{\mathrm{m}}$. For exchange reactions which are degenerate in the absence of intermolecular interactions $\overline{\Delta G}_{12}=0$.

3.5. Introduction of a two-dimensional site distribution function

At this stage we now have to take into account that different molecules in a given site m can experience different rate constants of the state exchange, although their equilibrium constant is the same. Thus, the introduction of subsites becomes necessary, i.e. the introduction of a two-dimensional distribution function $P(k_{1m2m}, K_{1m2m})$ or $P(k_{12}, K_{12})$. A function of the type $P(k_{1m2m}, k_{2m1m})$ or $P(k_{12}, k_{21})$ could also be introduced. The deviation of appropriate functions is facilitated if one assumes that kinetic and thermodynamic variables are not related. In this case the following product results

$$P(k_{1m2m}, K_{1m2m})=P(k_{1m2m})P(K_{1m2m})\,. \tag{38}$$

For the one-dimensional distribution function $P(k_{12})$ one could use according to Albery et al. [92] a Gaussian distribution of energies of activation $\Delta G_{12}^{\ddagger}$ of the kind

$$P(\Delta G_{12}^{\ddagger})=-\frac{1}{N}\frac{\mathrm{d}N}{\mathrm{d}\Delta G_{12}^{\ddagger}}=\frac{1}{2}\left(\frac{\alpha^{\ddagger}}{\pi}\right)^{1/2}\exp[-\gamma^{\ddagger}(\Delta G_{12}^{\ddagger}-\overline{\Delta G}_{12}^{\ddagger})^2]\,, \tag{39}$$

or

$$P(k_{12})=\frac{\mathrm{d}}{\mathrm{d}k_{12}}P(\Delta G_{12}^{\ddagger}),\quad k_{12}=\exp(-\Delta G_{12}^{\ddagger}/RT)\,. \tag{40}$$

Here, the usual superscript ‡ is introduced in order to distinguish the distribution parameters in eqs. (36) and (37). As an alternative to eq. (40), a Williams–Watts distribution [93] could be used.

3.6. Reduction of the two-dimensional distribution function to a one-dimensional function

We found that the above approach is difficult to realize experimentally because the above two-dimensional distribution function contain more parameters than can be derived by lineshapes analysis. A reduction of the two-dimensional distribution function to a one-dimensional function is, however, possible if one assumes a relationship between the thermodynamic and kinetic parameters, in contrast to eq. (38). Thus, let us assume a relationship of the type

$$k_{imjm}=K_{imjm}^{\alpha}k_{\mathrm{s}},\quad k_{jmim}=K_{imjm}^{\alpha-1}k_{\mathrm{s}}\,, \tag{41}$$

where k_{s} is the rate constant of the symmetric site with the equilibrium constant K_{imjm}, k_{imjm} the forward and k_{jmim} the backward rate constant. Eq. (41) resembles the Bronstedt equation which has been extensively used for the treatment of proton transfer [18]. For the case where $\alpha=0.5$, eq. (41) reduces to the simplest form of the well-known Marcus relation [25]. When $\alpha=1$, all backward rate constants k_{jmim} are equal to k_{s}. By combination with eq. (30) it follows that

$$k_{imjm}=k_{\mathrm{s}}\left(\frac{m-1}{l-1}\right)^{\alpha},\quad k_{jmim}=k_{\mathrm{s}}\left(\frac{m-1}{l-1}\right)^{\alpha-1}. \tag{42}$$

3.7. Calculated spectra in the presence of state exchange in the case of more than two superposed sites

Using a bi-Gaussian site distribution of free reaction enthalpies together with the approximation of eq. (42), we have calculated some theoretical spectra shown in fig. 5. In these calculations $l=16$ sites were taken into account. Whereas the site exchange rate constants were set to zero, the state exchange rate constants were increased from the bottom to the top. In the slow exchange region the spectra contain two sharp lines, as in the bottom spectra of fig. 3. As temperature is increased the lines show dynamic linebroadening and coalesce. In the fast exchange region the total spectrum consists of superposed individual sharp doublets with different spacings, as in the top spectrum of fig. 5. If the number of sites is increased this fine structure disappears and the resulting line is *inhomogeneously* broadened. For actual calculations it is only necessary to rise the number of sites until the difference between individual signals is smaller than their individual signal with W_0.

The main difference between the two sets of spectra in fig. 5 is that in fig. 5a we used the Marcus relationship with $\alpha=0.5$, whereas in fig 5b α was set to unity. Although one observes characteristic differences in the calculated lineshapes of both models in the two sets of spectra in fig. 5, one can anticipate that in experimental spectra it will probably not be easy to distinguish both models by lineshape analysis alone.

3.8. NMR lineshapes in the presence of site exchange

In this section we ask how exchange between the different sites affects the NMR spectra. In principle, the exchange operator given in eq. (16) covers a number of different exchange situations. The disadvantage of this operator is, however, that the site exchange rates depend on the arbitrary number of sites used in the calculations. Situations where the site exchange can be described by a single correlation time τ are, therefore, of special interest. The first simplification is to set

$$k_{imin}=k_{jmjn}=k_{mn} \tag{43}$$

in the exchange operator in eq. (16). Furthermore, one can assume that the rate constant k_{imin} is proportional to τ^{-1}, to the mole fraction x_n of site n, and to a parameter D_{mn}:

$$k_{mn}=\tau^{-1}x_nD_{mn}\,. \tag{44}$$

$D_{mn}=D_{nm}=0$ or 1 depending on whether exchange between sites m and n is allowed or not. From eq. (17) it follows for the inverse lifetime of an individual site that

$$\tau_m^{-1}=\sum_{r\neq m}k_{mr}=\tau^{-1}\sum_{r\neq m}x_rD_{mr}\,. \tag{45}$$

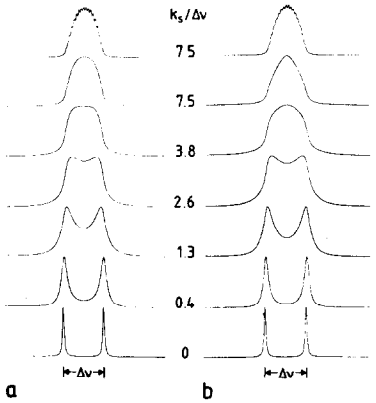

Fig. 5. Calculated spectra of bistable molecules located in a multitude of $l=16$ different sites, subject to exchange between the state. The sites were weight by a bi-Gaussian distribution function of free reaction energy. (a) Calculated spectra for the validity of Marcus theory, i.e. eq. (37) with $\alpha=0.5$. (b) Calculated spectra for the case that the backward rate constant is the same in all sites, i.e. eq. (37) with $\alpha=1$.

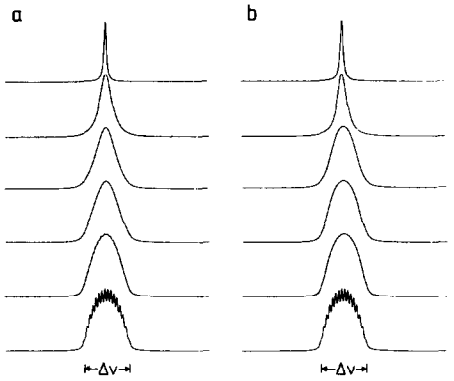

Fig. 6. Effects of a reduced site lifetime τ on the NMR spectra of bistable molecules located in different sites characterized by a bi-Gaussian distribution of free reaction energies of isomerism. The bottom spectrum where $\tau=\infty$ was generated in a similar way as the top spectrum in fig. 5. From the bottom to the top only the τ values were decreased. Fast site exchange renders all sites equivalent. (a) ASE model, (b) NSE model (see text). Reproduced with permission from ref. [6].

The elements of the exchange operator (eq. (16)) are then given by

$$\Xi_{imjn} = -\delta_{ij} \sum_{k \neq i} \delta_{mn} k_{imkn} + (1-\delta_{ij})\delta_{mn} k_{imjn} - \delta_{mn}\delta_{ij}\tau^{-1} \sum_{r \neq m} x_r D_{mr} + (1-\delta_{mn})\delta_{ij}\tau^{-1} x_n D_{mn} . \tag{46}$$

For the case of rapid state exchange this equation can be reduced to the operator given previously [5,6]

$$\Xi_{mn} = -\delta_{mn} \sum_{r \neq m} \tau_{si}^{-1} x_n D_{mr} + (1-\delta_{mn})\tau^{-1} x_n D_{mn} . \tag{47}$$

One can imagine two working hypothesis which represent two extreme limits of a complex exchange pattern. In limit (i) each site exchange with every other site, i.e. all $D_{mn}=1$, (ASE – all site exchange). Since $x_m \ll 1$ because of the great number of sites, it follows from eq. (45) that the lifetimes of all sites are equal, i.e. $\tau_m=\tau$. In limit (ii) each site exchanges only with a neighboring site, i.e. the equilibrium constants of state exchange change only gradually in small increments (NSE – neighbor site exchange). In other words, only values of D_{mn} with $m=n\pm 1$ are non-zero. In fig. 6 we compare the calculated NMR line shapes for both limits. In order to demonstrate better the effects of site exchange on the spectra we consider only 16 sites which leads to 16 separated lines at the bottom of figs. 6a and 6b where the average site lifetime $\tau\to\infty$. We use arbitrary site distribution. As we shorten τ, the homogeneous width of the individual lines first increases, leading to the disappearance of the fine structure, and then all individual lines coalesce into one homogeneously broadened line. In the fast site exchange regime only one sharp line survives. In the coalescence region the ASE model (fig. 6a) shows a "triangular" line shape, whereas the NSE line shape still resembles a Gaussian lineshape. In the slow and the fast exchange regime both models give rise to similar lineshapes and can, therefore, not be distinguished by one-dimensional NMR spectroscopy.

3.9. Computer program

In order to perform the lineshape calculations based on the theory presented in this section a computer program was written in FORTRAN 77. The program requires the matrix $\mathcal{M}$, the vector $\rho(0)$ defined in eqs. (1)–(7), i.e. the quantities $\Delta\nu$, σ, α, ΔG_{12}^{m}, W_0, τ^{-1}, and D_{mn}, defined above as input. The inhomogeneously broadened spectra in the absence of site exchange shown in fig. 5 were calculated by setting $\tau^{-1}=0$.

4. Results

In this section we present the results of our ^{15}N and ^{13}C variable temperature CPMAS NMR experiments performed on the crystalline α and β modifications and a novel amorphous modification of phthalocyanine (Pc). Some of these results have been presented previously in a preliminary form [16,49].

4.1. ^{15}N CPMAS NMR studies of crystalline α- and β-Pc

Fig. 7 shows the superposed experimental and calculated ^{15}N CPMAS NMR spectra of α- and β-Pc as a function of temperature. Characteristic temperature-dependent lineshape changes in these spectra indicate a mobility of the central protons. Below 173 K two narrow ^{15}N lines with an intensity ratio of approximately 3:1 are observed. The smaller high field line originates from the central ^{15}N atoms bound to hydrogen atoms, the low field line from the six unprotonated nitrogen atoms. At higher temperatures only the four outer nitrogen atoms which do not participate in the tautomerism contribute to the low field line. In the β modification this line is split into two singlets which indicates the presence of two inequivalent pairs of outer nitrogen atoms. By contrast, this splitting is absent in the α modification, indicating that within the margin of error of our NMR experiments the outer nitrogen atoms are equivalent. This equivalence may be only a quasi-equivalence, because the low-field line is slightly broader than the corresponding line components of the β phase, i.e. the α phase may contain a distribution of slightly inequivalent outer nitrogen atoms.

If temperature is raised dynamic line broadening and coalescence of the signals of the inner $^{15}N_4$ core are observed. The observation of two sharp coalesced lines with a temperature-dependent reduced splitting $\delta\nu$ can easily be interpreted in terms of the calculated line shapes shown at the bottom of fig. 3. This result indicates that the degeneracy of the two tautomers is lifted in this modification, due to molecular packing effects. In other words, the spectra prove that one tautomeric form is energetically favored over the other. From the values of $\delta\nu$ the equilibrium constants K_{12} of the tautomerism could be calculated as a function of temperature using eq. (28). We obtain a reaction enthalpy of $\Delta H_{12}=1.3\pm0.2$ kJ mol^{-1} and a reaction entropy of $\Delta S_{12}=0.8$ J K^{-1} mol^{-1}. The rate constants k_{12} were obtained by the simulation of the spectra. The K_{12} values necessary for these calculations were extrapolated from high temperature. The linewidths W_0 in the absence of exchange were obtained by simulation of the signals of the outer nitrogen atoms. We obtained the following Arrhenius equation

$$k_{12}=10^{11.3\pm0.5}\exp(-32.3\pm1.6\ \text{kJ mol}^{-1}/RT),\quad 167\leqslant T\leqslant 213\ \text{K},\quad k(298)\approx 0.43\times10^{6}\ \text{s}^{-1}. \tag{48}$$

All further kinetic and thermodynamic parameters are summarized in tables 1 and 2.

By contrast, the high temperature ^{15}N spectra of the α modification contain only one slightly broadened resonance for the inner $^{15}N_4$ core. This additional broadening might be explained by one of the following working hypotheses: (i) the signal consists of two non-resolved lines with a small splitting $\delta\nu$ arising from an equilibrium constant close to but not exactly unity; (ii) the broadening is the consequence of a narrow distribution of different $\delta\nu$ values, i.e. equilibrium constants with a mean value of $K_{12}=1$; (iii) a susceptibility broadening

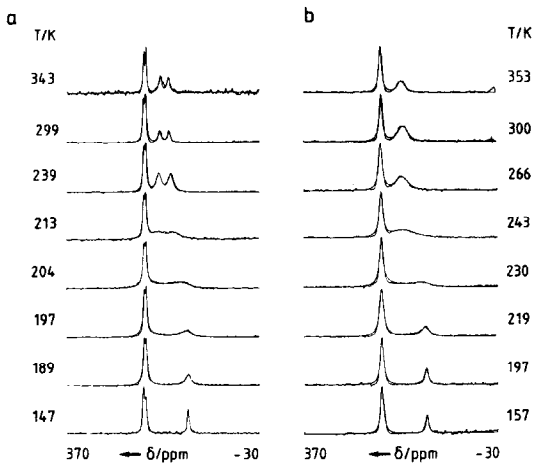

Fig. 7. Supposed experimental and calculated ^{15}N CPMAS NMR spectra of 95% ^{15}N enriched phthalocyanine as a function of temperature. (a) β modification: 10–12 ms cross polarization time, 7 kHz sweep width, 2.7 s repetition time, reference external $^{15}NH_4Cl$. (b) α modification: same acquisition parameters as in (a).

Table 1
Equilibrium constants of tautomerism in β-phthalocyanine

T (K)	$\delta\nu$ (Hz)	K_{12}
292	185	0.639
309	180	0.647
324	171	0.663
355	147	0.704
150	844 [a]	

[a] Low temperature splitting $\Delta\nu$ in the absence of proton transfer.

Table 2
Forward rate constants of the tautomerism of β-phthalocyanine [a]

T (K)	k_{12} (s^{-1})
167	20
175	44
183	116
189	185
193	220
197	600
204	1240
209	1690
213	2800

[a] Simulations parameters: $\Delta\nu = 844$ Hz, $W_0 = 40$ Hz.

could also be present in view of the fact that the α-Pc crystals are very small. In any case, one can conclude that the proton migration in the α modification proceeds in good approximation along a quasi-symmetrical double minimum potential. Therefore, we set in the lineshape calculations of fig. 7 the equilibrium constant $K_{12} = 1$ in the whole temperature range, i.e. $k_{12} = k_{21} = k_s$. Thus, we obtained the following rate constants:

$$k_s = 10^{12.0 \pm 0.2} \exp(-39.8 \pm 0.9 \text{ kJ mol}^{-1}/RT), \quad 197 \leqslant T \leqslant 243 \text{ K}, \quad k_s(298 \text{ K}) \approx 0.11 \times 10^6 \text{ s}^{-1}. \tag{49}$$

All kinetic data are summarized in table 3.

4.2. ^{13}C CPMAS studies of phthalocyanine

In order to know whether it is possible to easily distinguish α- and β-phthalocyanine by routine ^{13}C NMR spectroscopy and in order to obtain additional information on the molecular structure and dynamics of both modifications we have measured the ^{13}C CPMAS NMR spectra of ^{15}N labeled Pc shown in fig. 8. Obviously, the spectra are temperature dependent because of the proton tautomerism. The spectral pattern of the NMR signals of the α phase (fig. 8b) follows the one described by Meier et al. [54]. At low temperature we observe in the

Table 3
Rate constants of the tautomerism of α-phthalocyanine [a]

T (K)	k (s^{-1})
197	30
204	65
219	300
230	1050
243	2780

[a] Simulations parameters: $\Delta\nu = 844$ Hz, $W_0 = 61$ Hz.

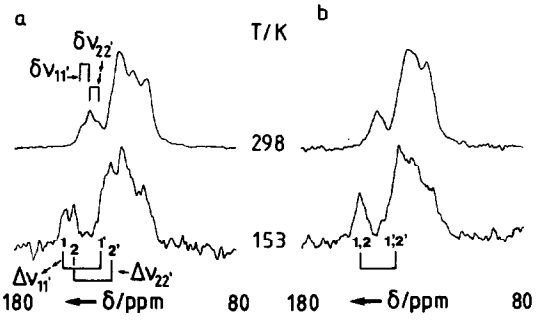

Fig. 8. ^{13}C CPMAS NMR spectra of 95% ^{15}N enriched phthalocyanine at 22.63 MHz at 298 and 153 K. (a) β modification, (b) α modification. The spectra were obtained with a 7 mm Doty-spinner design [91] in a cryomagnet. 3–6 ms CP time, 4.7 s repetition time, 4 μs 90° time, 5 kHz spectra width, 3 kHz rotation frequency on average, reference TMS.

low field region one broad single resonance labeled as 1, 2 at 154 ppm. This chemical shift is typical for carbon atoms in the positions neighboring the unprotonated nitrogen atoms of porphyrins. At room temperature one slightly broadened coalesced signal is observed at 146 ppm. From the position of this averaged signal one can easily calculate the chemical shifts of the signals 1′ and 2′ hidden under the large high field peak. We obtain a value of 138 ppm, which agrees well with the value of Meier et al. [54].

By contrast, in the β modification (fig. 8a) two singlets are observed in the low-temperature spectrum at 156 and 152 ppm, indicating the presence of two inequivalent carbon atoms adjacent to unprotonated inner nitrogen atoms. At room temperature, where the proton transfer is fast, the β modification gives rise to a trio of lines at 149.5, 146 and 142.5 ppm with an intensity ratio of 1 : 2 : 1. As shown in fig. 8a, the formation of this trio is easily explained in terms of two superposed line pairs characterized by the reduced splittings $\delta\nu_{11'} \approx \delta_{22'}$. As in the ^{15}N spectra these reduced splittings arise from an equilibrium constant of tautomerism of $K_{12} \neq 1$. Since the K_{12} values were already known from the ^{15}N spectra (table 1), we were able to calculate the intrinsic chemical shifts of the carbon atoms leading to lines 1′ and 2′. We obtain the values of 140 and 136.5 ppm.

4.3. ^{15}N CPMAS NMR studies of amorphous phthalocyanine

The ^{15}N CPMAS NMR spectra of the amorphous modification of phthalocyanine which we denote as am-Pc show surprising differences when compared to the spectra of the α and the β modifications. In fact, the amorphous nature of am-Pc was established by recording the spectra shown in fig. 9. At low temperatures the familiar phthalocyanine spectrum consisting of two lines with the intensity ratio of 3:1 in the slow proton exchange regime is obtained. The spectral assignment is the same as reported above for the crystalline modification. Lowering the temperature did not result in line narrowing. Raising the temperature led again to dynamic line broadening of the inner $^{15}N_4$ atom signal. However, in contrast to the spectra in fig. 7, we do not observe line narrowing above 250 K but a very broad line with a characteristic temperature dependence. In order to elucidate whether this broadening is homogeneous, i.e. arising from dynamic processes or whether it is inhomogeneous, i.e. arising from a superposition of sharp lines as indicated in fig. 5, a two-dimensional exchange experiment at room temperature was performed [38]. Complications arising from spin diffusion and longitudinal relaxation arising from the proton dynamics [94] were avoided by limiting the mixing time to 250 ms. The two-dimensional ^{15}N CPMAS NMR spectrum in fig. 10 shows a narrow ridge along the diagonal, as expected for a superposition of individual sharp lines. Otherwise, if the line had been homogeneously broadened, the two-dimensional signal would extend in a similar way in both frequency axes, i.e. exhibit a circular shape [38].

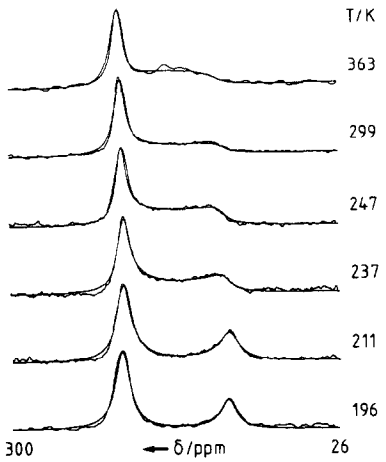

Fig. 9. Superposed experimental and calculated ^{15}N CPMAS NMR spectra of amorphous phthalocyanine as a function of temperature. 6–12 ms CP time, 2.7 s repetition rate, 3000 scans on the average, reference external $^{15}NH_4Cl$.

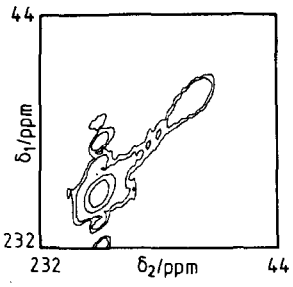

Fig. 10. Two-dimensional magnetization transfer ^{15}N CPMAS NMR spectra (contour plot) at 300 K of amorphous phthalocyanine. There were 32 by 256 points in the original data matrix. 6 ms CP time, 250 ms mixing time, 3.1. s repetition rate, 512 scans per spectrum, reference external $^{15}NH_4Cl$.

Table 4
Thermodynamic and kinetic parameters of tautomerism in amorphous phthalocyanine [a)]

T (K)	A (kJ/mol)	σ (kJ/mol)	τ_{st}^{-1} (s^{-1})
196	3.75	3.20	≈25
211	3.21	2.94	140
237	3.17	3.12	1690
240	3.11	3.00	2175
247	2.93	3.03	3830
255	2.86	3.06	7030
299	2.16	3.06	≈110000
339	2.13	3.08	$\approx 0.7\times10^6$
363	1.54	3.02	$\approx 2\times10^6$

[a)] Simulation parameters: $\Delta\nu = 820$ Hz, $W_0 = 100$ Hz. $l = 16$ sites were considered.

The origin of the inhomogeneous line broadening at high temperature can be explained in terms of the theory presented in sections 3.4–3.7 with a continuous distribution of different sites in which the Pc molecules experience different equilibrium and rate constants of tautomerism. This distribution of sites implies the breakdown of the ordered crystal lattice. The spectra in fig. 9 were simulated by taking into account a bi-Gaussian distribution of the free energy of tautomerism $P(\Delta G)$. The symmetry of the phthalocyanine molecule was taken into account by setting the mean value of $\overline{\Delta G}_{12} = 0$ in eq. (37), i.e. the mean equilibrium constant $\bar{K}_{12} = 1$. In order to avoid the use of a two-dimensional distribution function $P(K_{12}, k_{12})$ and to simplify the calculations, eq. (42) was employed to simulate the spectra in fig. 9, with a value of $\alpha = 0.5$, corresponding to the Marcus relationship [25]. In order to further reduce the number of variable parameters we used the symmetrical state exchange rate constants k_s of the α modification, given in eq. (49). Thus, only the parameters ΔG_{12}^m and σ of the Gaussian distribution function (eq. (37)) needed to be adapted. ΔG_{12}^m is the free energy of tautomerism of the most probable site. The results are listed in table 4. From the equation $\Delta G_{12}^m = \Delta H_{12}^m - T\Delta S_{12}^m$, a reaction enthalpy $\Delta H_{12}^m = 5.9 \pm 0.3$ kJ mol^{-1} and a reaction entropy $\Delta S_{12}^m = 12.1 \pm 1.1$ J K^{-1} mol^{-1} of the most probable site were obtained.

5. Discussion

Let us first summarize the main results of this study. Using dynamic high-resolution ^{15}N and ^{13}C solid state NMR spectroscopy of ^{15}N labeled phthalocyanine (Pc) in the crystalline α and β modifications (fig. 7) as well as of a novel amorphous modification (fig. 9), it was established that Pc is subject in the solid state to an intramolecular double-proton transfer according to fig. 1. Because of the insolubility of this dye in organic solvents this tautomerism could not be detected previously by conventional liquid state NMR techniques. The energy surface of the tautomerism depends on the environment in which the molecule is placed. Whereas the tautomers are quasi-degenerate in the thermodynamically less stable α modification, the degeneracy of the tautomerism is lifted in the case of β-Pc. The equilibrium constant of tautomerism of β-Pc is $K_{12} = 0.65$ at room temperature. In addition, the two carbon atoms adjacent to the nitrogen atoms are no longer equivalent in contrast to the α phase. The amorphous modification which may contain defects generated by decomposition of Pc is characterized by a broad distribution of equilibrium constants K_{12}. Besides thermodynamic differences, the various modifications also show interesting differences in the proton transfer dynamics. Proton transfer in

the β phase is faster than in the α phase due to a smaller energy of activation, i.e. $E_a(\beta) < E_a(\alpha)$. In addition, we also found that the frequency factor of proton transfer in the β phase is smaller than in the α phase. For the amorphous modification as well a broad distribution of rate constants is observed. In order to extract the thermodynamic and the kinetic information by lineshape analysis, a previous NMR lineshape theory of bistable molecules exchanging between two molecular states, embedded in ordered and disordered matrices, was further developed to include the case of slow state exchange.

These results show that there is a subtle interplay between intermolecular interactions, the intramolecular structure, and the proton transfer characteristics discussed in the following.

5.1. The structure of phthalocyanine in the solid state

In order to discuss the effects of the environment on the Pc tautomerism let us first review some structural features of Pc in the solid state relevant for this study. We are especially interested in the arrangement of the inner nitrogen atoms. In order to facilitate the discussion we show in fig. 11 the atom numbering to which we refer in the following.

The best known Pc modification is the monoclinic β phase whose molecular symmetry is only $\bar{1}$ [78]. The inner nitrogen atoms a to d are located on a rectangle with the distances $r_{ab} \approx r_{cd} \approx 265$ Å $< r_{ac} \approx r_{bd} \approx 2.75$ Å, as indicated in fig. 11. This deviation from a square arrangement of the inner nitrogen atoms is independently supported by our NMR experiments. Firstly, the two low field ^{15}N signals of fig. 7a indicate the presence of two different kinds of outer nitrogen atoms. Secondly, we observe that the two carbon neighbors 1 and 2 as well as 1′ and 2′ of each inner nitrogen atom have different chemical shifts. These results are not consistent with a square arrangement of the inner and the outer N atoms. The assignment of these ^{13}C lines to atom positions is indicated in fig. 11. Note that the data are also in agreement with an assignment where 1 and 2 as well as 1′ and 2′ are interchanged.

Unfortunately, no exact structural data are available for the α modification because this material could be obtained only as a microcrystalline powder insufficient for X-ray analysis [86]. There is, however, some evidence from X-ray diffraction investigations that the molecular symmetry of the α phase might be higher than that of the β modification [82–86]. This evidence is supported by our NMR experiments. The latter indicate a chemical equivalence of the outer nitrogen atoms, of carbon atoms 1 and 2 as well as of carbon atoms 1′ and 2′

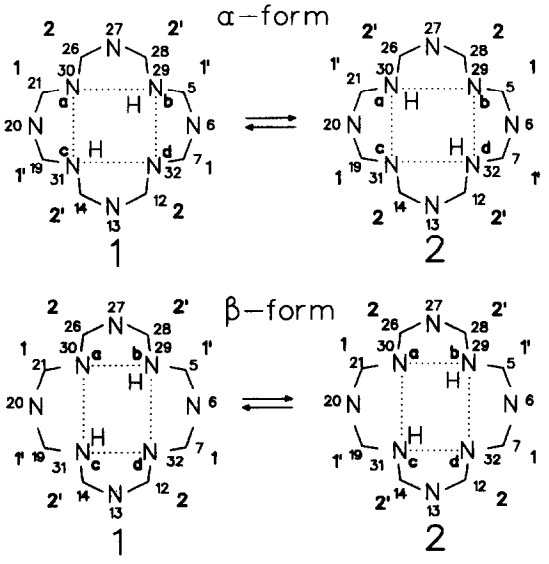

Fig. 11. Schematic representation of the geometry of phthalocyanine in the solid state. The boldfaced symbols are used in the context of this study for atom numbering; for comparison also the IUPAC [95] numbering is shown.

at low temperature, as expected for a square arrangement of the inner and outer nitrogen atoms. Thus, the distances between the inner nitrogen atoms are more or less equal; one can assume that $r_{ab} \approx r_{cd} \approx r_{ac} \approx r_{bd} \approx 2.7$ Å, which corresponds to the average distance in the β phase.

No structural X-ray or neutron scattering data are available for the amorphous form found during this study. Although no impurity could be detected in the ^{15}N spectra shown in fig. 9, we cannot exclude that this form contains a number of defects generated during the annealing process.

5.2. *Influence of the environment on the thermodynamics of the Pc tautomerism*

Let us discuss now how the different molecular structures influence the tautomerism in solid Pc. In the absence of intermolecular interactions the two tautomers in scheme 1 are degenerate, i.e. the equilibrium constant K_{12} of the reaction is unity.

5.2.1. *Crystalline α and β modifications*

The lineshape analysis of the ^{15}N CPMAS NMR spectra of monoclinic β-Pc (fig. 7a) shows that the degeneracy of the tautomers is lifted in this modification. In other words, the hydrogen migration proceeds along a slightly asymmetric potential energy surface. This finding can be understood in terms of the reduced crystal symmetry of the β phase. Thus, the two tautomers in the unit cell are no longer related by symmetry operations and it is understandable that their degeneracy is lost. Note that this loss of degeneracy of the two tautomeric forms is also proof that the molecules in β-Pc are not able to perform 90° jumps around an axis perpendicular to the molecular plane within the NMR timescale. Such a rotation would lead to an exchange of the nitrogen sites, i.e. to a coalescence of the two remaining lines in the fast proton exchange regime, according to the calculated spectra of fig. 3.

For the α phase we find that the two tautomers are quasi-degenerate, which corresponds well with our finding of a higher molecular symmetry as compared to the β phase. The NMR lines of the inner ^{15}N atoms of this compound (fig. 7b) are, however, slightly broader than the corresponding lines of the β phase. There may be different sources for this additional line broadening. Either the deviation of the equilibrium constants of tautomerism, K_{12}, from unity is too small to be observable or there is a narrow distribution of slightly different values of K_{12} and of the chemical shifts as a consequence of some crystal defects in this phase, or the broadening is a consequence of the smallness of the crystals of α-Pc. In contrast to the β phase, it cannot be completely excluded that the observed quasi-degeneracy of the two tautomers in the α phase partly arises from molecular 90° jumps, although this possibility seems unlikely.

The common property of the two crystalline Pc modifications is, that all molecules in a given phase experience the same equilibrium constants of tautomerism because of long range ordering in the crystalline state.

5.2.2. *Amorphous phthalocyanine*

The situation changes if the long range order of the solid matrix breaks down, which is realized e.g. in glassy polymers or in the bulk material of an amorphous compound. Optical investigations of porphyrins and phthalocyanine showed that a disordered solid matrix provides a multitude of different environments in which the hosts experience different electronic transition frequencies [65–69].

In a previous article we investigated the tautomerism of an organic dye molecule embedded in a glassy polymer [5,6]. It was found that this matrix provides different sites in which the dye molecules experience different equilibrium constants of tautomerism. A similar observation is made here for the case of amorphous Pc, where the bulk dye provides its own disordered matrix. This information follows from the analysis of the ^{15}N NMR lineshape of am-Pc in the fast proton exchange regime at high temperature, where one broad line is observed for the inner nitrogen atoms. Two-dimensional exchange experiments (fig. 10) reveal a narrow ridge along the diagonal axis which is proof that the line is inhomogeneously broadened, i.e. that it consists of a superposition of doublets with different splittings due to different local equilibrium constant, as explained in section 3. This

broad distribution is the consequence of the fact that the periodicity of the crystal lattice has been lost in the amorphous state.

The observed distribution of equilibrium constants of tautomerism means that a distribution of free reaction energies or enthalpies of tautomerism exists too. In order to simulate the NMR lineshapes, a bi-Gaussian distribution function of free reaction enthalpy $P(\Delta G_{12})$ was used, with a mean value of $\overline{\Delta G}_{12}=0$, i.e. a mean equilibrium constant of $\bar{K}_{12}=1$, because of the molecular symmetry in the absence of intermolecular interactions. The distribution is characterized by the parameters ΔG^{m} and σ. ΔG^{m} represents the most probable reaction enthalpy and σ the width of the distribution.

Again, as in the case of β-Pc, we can exclude the possibility that the Pc molecules perform 90° jumps around an axis perpendicular to the molecular plane. In this case the broad high-temperature line in fig. 7a would coalesce into one single line, as shown in the calculated spectra of fig. 3.

5.3. Influence of the environment on the kinetic of the Pc tautomerism

So far we have discussed perturbations of reactant and product states of the tautomerism by the interplay of intermolecular and intramolecular interactions. In this section we show that such perturbations exist also for the transition states of the Pc tautomerism.

5.3.1. Crystalline α and β modifications: evidence for proton tunneling

The Arrhenius curves of the proton transfer in both α- and β-Pc are shown in fig. 12. Our values found for α-Pc agree very well with those Meier et al. [54] determined by ^{13}C NMR spectroscopy. Fig. 12 clearly shows that the reaction is much faster in β-Pc than in α-Pc due to a smaller energy of activation (32.3 kJ mol^{-1} versus 39 kJ mol^{-1}), as expressed by eqs. (48) and (49). Also, the frequency factor is smaller for the β modification.

An explanation for the different behavior of both phases may be provided by the following arguments. It is well known that the barrier for proton transfer between two heavy atoms increases with the internuclear distance [2]. The different kinetic behavior of both modifications can then be explained by the possibility that the proton transfer in the β phase proceeds preferentially between the two nitrogen atoms with the shorter interatomic distance. Proton migration to the more distant nitrogen atoms will be characterized by a higher energy of activation. The latter process does, however, not lead to further lineshape changes in the ^{15}N spectra. By contrast, as stated above, in the case of α-Pc the inner nitrogen atoms are arranged in a good approximation on a square, the average nitrogen distance being larger than the shortest nitrogen distance in β-Pc, which might explain the larger energy of activation of the proton transfer in this phase.

The different apparent frequency factors of the proton motion in both phases can be interpreted in terms of substantial tunneling contributions to the reaction rates of proton transfer, especially to those of the β phase.

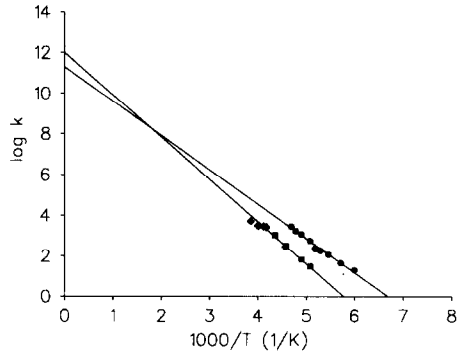

Fig. 12. The Arrhenius curves of α- and β-Pc according to eqs. (48) and (49). (●) β-Pc this study, (■) α-Pc this study, (♦) α-Pc ref. [54].

This can be visualized as follows. Extrapolation of the Arrhenius curves in fig. 12 to the high-temperature region predicts that above 600 K proton transfer in the α phase will be faster than in the β phase, which is unlikely (48). Preliminary tunnel calculations [19] using frequency factors of 10^{13} s^{-1} indicate a curvature in the Arrhenius curve of the β phase and a high-temperature activation energy of about 40 kJ mol^{-1}. These calculations also show that an additional reason for the faster proton transfer in the β phase might be a lower energy of a possible intermediate with protons attached to adjacent nitrogen atoms. However, in order to verify this interpretation further NMR experiments will be necessary, especially the determination of kinetic isotope effects in the widest temperature range possible. Optical methods might also help to achieve this goal [56].

5.3.2. Amorphous phthalocyanine

The ^{15}N CPMAS NMR spectra of am-Pc (fig. 9) indicate that the proton transfer in this compound is frozen at low temperatures within the NMR timescale, as in the case of the crystalline Pc modifications. As temperature is raised lineshape changes in the intermediate proton exchange region provide information about proton dynamics and thermodynamics of tautomerism as well. In principle, two-dimensional distributions of rate constants $P(k_{12}, k_{21})$ have to be considered. However, in the case of am-Pc the lineshapes did not provide enough information to obtain such a two-dimensional distribution function experimentally. A reduction to a one-dimensional distribution function can be achieved by assuming a Bronstedt type relationship between rate and equilibrium constants of the type $k_{12}=K^{\alpha}k_s$. k_s is the rate constant of the symmetric double-minimum potential with $K=1$. The case where $\alpha=0.5$ represents the well known Marcus relationship for intermolecular reaction. When $\alpha=1$ all backward rate constants are set to the same value k_s. Our spectra could be well simulated with $\alpha=0.5$. In order to further minimize the number of variable parameters we took the values of k_s from those found for α-Pc. Thus, only the width σ of the distribution function $P(\Delta G_{12})$ and the most probable free energy of tautomerism $\Delta G^{m}_{12}=\Delta H^{m}_{12}-T\Delta S^{m}_{12}$ were varied in the lineshape simulations. We found values of $\sigma=3$ kJ mol^{-1}, a mean reaction enthalpy of $\Delta H^{m}_{12}=5.9$ J mol^{-1} and a reaction entropy of $\Delta S^{m}_{12}=12$ J $kmol^{-1}$.

5.4. Implications for the mechanism of hydrogen transfer reactions in condensed matter

Let us finally discuss the implications of the above findings for the mechanism of hydrogen transfer reactions in condensed matter. In fig. 13 we present a molecular picture of the influence of intermolecular interactions on this type of reaction. This picture partly arose from our studies of dye tautomerism in organic glasses such as polystyrene [5,6]. Consider a bistable molecule in the gas phase which has access to two degenerate molecular states (fig. 13a). The energy profile along the reaction coordinate will then correspond in the simplest case to a symmetric double-minimum potential. If the molecule is placed in a crystalline environment on a site of reduced symmetry, the degeneracy of the two molecular states will be lost because an energy difference exists between the two states (fig. 13b). In the case of small perturbations the entropy difference between the two states may be small. Thus, small deviations of the equilibrium constants from unity are expected, which increase, however, at very low temperatures. In first approximation the local equilibrium constant of a given molecules does not depend on the molecular state of the neighboring molecule. Otherwise, a second-order phase transition is expected at higher temperatures, absent in the case of Pc. The energy difference between the two states depends on the subtle interplay between the molecular structure and the intermolecular interactions. Thus, different perturbations of the energy reaction surface must be expected for different environments, as in the case of α- and β-Pc. Not only the energy difference between the reactant and product states is varied but also the barrier height found here.

If the molecule is placed in a disordered environment its reaction energy surface will be dependent on the local environment (fig. 13c). Thus, the overall reaction must be characterized by a large distribution of rate and equilibrium constants, as observed here for am-Pc. In our previous studies of dye tautomerism in glassy polymers [5,6] we only observed distributions of equilibrium constants. Information on this distribution can be obtained by NMR methods. In section 3 it is shown how solvent relaxation via molecular motions leads to a

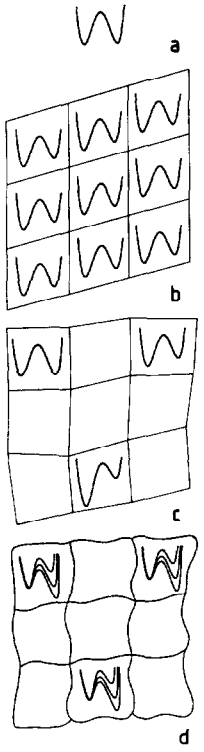

Fig. 13. Perturbation of a symmetric double-minimum potential of a bistable molecule by intermolecular interactions. (a) Symmetric double-minimum potential in the gas phase. (b) Perturbation of the potential in the ordered crystalline state by intermolecular interactions which are the same for all molecules. (c) Perturbation of the potential in the disordered solid state by intermolecular interactions which are different for all molecules. (d) Motional averaged symmetric potentials. (Adapted from ref. [6].)

motional averaging of the observed energy reaction surfaces in a regime where dynamic NMR spectroscopy can no longer follow the individual reaction sites (fig. 13d). Then, in the case of symmetric bistable molecules such as Pc only averaged symmetric double minimum potentials are observed. This regime has not yet been reached in the case of solid Pc in the temperature range studied; however, this regime was recently [5,6] achieved in the case of dyes embedded in glassy polymers above the glass transition temperature.

The example of different proton transfer characteristics in the various phases of phthalocyanine together with the results of this section shows that extreme care has to be taken when one tries to construct and interpret the Arrhenius curve of a given reaction in a wide temperature range when the kinetic data have been derived from different phases e.g. liquid, solid, solid solutions. In order to do so it must be checked whether there are kinetic liquid/solid state effects and how they influence the reaction dynamics. This has been achieved in the case of the tautomerism of porphyrin by NMR spectroscopy [50,56].

6. Conclusions

It has been shown that dynamic solid state NMR spectroscopy can be very helpful in understanding fast reactions in bistable molecules embedded in the ordered or disordered solid state where the timescale of slow molecular motion is reached by this method. Thus, information about the question of how sensitive reacting molecules respond to intermolecular interactions can be obtained, as shown here for crystalline and amorphous phthalocyanine. Since the amorphous solid state and, especially, the glassy state can be regarded as a model for liquids in a timescale of slow solvent motion we think that our results may also be useful in the understanding of fast reactions in liquids. Thus, we have shown that molecules in different local environments are not only

characterized by a Gaussian distribution of different microscopic rate constants but also of different microscopic equilibrium constants. The assumption of relations between thermodynamic and kinetic quantities is useful for the evaluation of the experimental data. Although in this study we have not yet measured kinetic hydrogen/deuterium isotope effects of the Pc tautomerism, we have already found evidence for major tunneling contributions to the reaction rates, especially to those of β-Pc. One can anticipate that NMR studies of bistable molecules in solids may not only lead to a better theoretical understanding of reactions in condensed matter but may also be of technical importance in the field of material research. Tasks for the future include further exploiting the whole spectrum of one- and two-dimensional solid state NMR techniques in order to achieve this goal.

Acknowledgement

We thank the Stiftung Volkswagenwerk, Hannover, the Deutsche Forschungsgemeinschaft, Bonn-Bad Godesberg and the Fonds der Chemischen Industrie, Frankfurt, for financial support. Stimulating discussions with Dr. C.S. Yannoni, IBM Almaden Research Center, San Jose, USA, are gratefully acknowledged.

References

[1] H.S. Johnston, Gas Phase Reaction Rate Theory (Ronald Press, New York, 1966).
[2] P. Schuster, G. Zundel and C. Sandorfy, eds. The Hydrogen Bond–Recent Developments in Theory and Experiments (North-Holland, Amsterdam, 1976).
[3] W. Siebrand and T.A. Wildman, Accounts Chem. Res. 19 (1986) 238.
[4] P.F. Barbara and W. Jarzebe, Accounts Chem. Res. 21 (1988) 195.
[5] B. Wehrle, H. Zimmermann and H.H. Limbach, Ber. Bunsenges. Physik. Chem. 91 (1987) 941.
[6] B. Wehrle, H. Zimmermann and H.H. Limbach, J. Am. Chem. Soc. 110 (1988) 7014.
[7] A. Abragam, Principles of Nuclear Magnetism (Oxford Univ. Press, Oxford, 1961).
[8] H.S. Gutowsky, D.M. McCall and C.P. Slichter, J. Chem. Phys. 21 (1953) 279.
[9] R. Kubo, Nuovo Cimento Suppl. 6 (1957) 1063;
R.A. Sack, Mol. Phys. 1 (1958) 163.
[10] G. Binsch, J. Am. Chem. Soc. 91 (1969) 1304.
[11] H.H. Limbach, J. Magn. Reson. 36 (1979) 287.
[12] R.R. Ernst, G. Bodenhausem and A. Wokaun, Principles of Nuclear Magnetic Resonance in One and Two Dimensions (Clarendon Press, Oxford, 1987).
[13] J. Schaeffer and E.O. Stejskal, J. Am. Chem. Soc. 98 (1976) 1031.
[14] C.A. Fyfe, Solid State NMR for Chemists (CFC Press, Guelph, 1983) and references cited therein.
[15] J.R. Lyerla, C.S. Yannoni and C.A. Fyfe, Accounts Chem. Res. 15 (1982) 208.
[16] R.D. Kendrick, S. Friedrich, B. Wehrle, H.H. Limbach and C.S. Yannoni, J. Magn. Reson. 65 (1985) 159.
[17] G. Kämpf, Ber. Bunsenges. Physik. Chem. 89 (1985) 1179.
[18] R.P. Bell, The Proton in Chemistry, 2nd Ed. (Chapman and Hall, London, 1973).
[19] R.P. Bell, The Tunnel Effect in Chemistry (Chapman and Hall, London, 1980).
[20] E.F. Caldin and V. Gold, Proton Transfer Reactions (Chapman and Hall, London 1975).
[21] J. Brickmann and H. Zimmermann, Ber. Bunsenges. Physik. Chem. 70 (1966) 157; 70 (1966) 521; 71 (1971) 160.
[22] J. Brickmann and H. Zimmermann, J. Chem. Phys. 50 (1969) 1608.
[23] J. Brickmann, Ber. Bunsenges. Physik. Chem. 84 (1980) 186.
[24] M. Klöffler and J. Brickmann, Ber. Bunsenges. Physik. Chem. 86 (1982) 203.
[25] R.H. Marcus, J. Phys. Chem. 72 (1986) 891.
[26] H.H. Limbach, The Use of NMR Spectroscopy in the Study of Hydrogen Bonding in Solution, in: Aggregation Processes, eds. J. Gormally and E. Wyn-Jones (Amsterdam, Elsevier, 1983) ch. 16.
[27] C.B. Storm and Y. Teklu, J. Am. Chem. Soc. 94 (1974) 53; Ann. NY Acad. Sci. 206 (1973) 631.
[28] H.H. Limbach, L. Meschede and G. Scherer, Z. Naturforsch., in press.
[29] H.H. Limbach, J. Hennig, D. Gerritzen and H. Rumpel, Faraday Discussions Chem. Soc. 74 (1982) 822.
[30] J. Hennig and H.H. Limbach, J. Am. Chem. Soc. 106 (1984) 292.
[31] D. Gerritzen and H.H. Limbach, J. Am. Chem. Soc. 106 (1984) 869.

[32] M. Schlabach, B. Wehrle, H.H. Limbach, E. Bunnenberg, A. Knierzinger, A.Y.L. Shu, B.R. Tolf and C. Djerassi, C. J. Am. Chem. Soc. 108 (1986) 3856.
[33] M.J. Crosswell, L.D. Field, M.M. Harding and S. Sternhell, J. Am. Chem. Soc. 109 (1987) 2335.
[34] G. Otting, H. Rumpel, L. Meschede, G. Scherer and H.H. Limbach, Ber. Bunsenges. Physik. Chem. 90 (1986) 1122.
[35] L. Meschede, D. Gerritzen and H.H. Limbach, Ber. Bunsenges. Physik. Chem. 92 (1988) 469.
[36] M. Schlabach, H. Rumpel and H.H. Limbach, Angew. Chem. 101 (1989) 84; Angew. Chem. Intern. Ed. 28 (1989) 76.
[37] H. Rumpel and H.H. Limbach, J. Am. Chem. Soc., in press.
[38] N.M. Szeverenyi, M.J. Sullivan and G.E. Maciel, J. Magn. Reson. 47 (182) 462.
[39] W.I. Shiau, E.N. Duesler, I.C. Paul, D.Y. Curtin, W.G. Blann and C.A. Fyfe, J. Am. Chem. Soc. 105 (1983) 2579.
[40] N.M. Szeverenyi, A. Bax and G.E. Maciel, J. Am. Chem. Soc. 105 (1983) 2579.
[41] P.C. Myrrhe, J.D. Kruger, B.L. Hammond, S.M. Lok, C.S. Yannoni, V. Macho, H.H. Limbach and H.M. Vieth, J. Am. Chem. Soc. 106 (1984) 6079.
[42] A. Baldy, J. Elguero, R. Faure, M. Pierrot and E.J. Vincent, J. Am. Chem. Soc. 107 (1985) 5290.
[43] B. Wehrle, F. Aguilar, H.H. Limbach, M.C. Foces-Foces, F.H. Cano, J. Elguero, A. Baldy, M. Pierrot, M.M.T. Khurshid, J.B. Larcombe-McDouall and J.A.S. Smith, J. Am. Chem. Soc., submitted for publication.
[44] H.H. Limbach, B. Wehrle, M. Schlabach, R.D. Kendrick and C.S. Yannoni, J. Magn. Reson. 77 (1988) 84.
[45] F. Graf, R. Meyer, T.K. Ha and R.R. Ernst, J. Chem. Phys. 75 (1982) 2914.
[46] S. Nagaoka, T. Terao, F. Imashiro, A. Saika, A.N. Hirota and S. Hayashi, Chem. Phys. Letters 80 (1981) 580; J. Chem. Phys. 79 (1983) 4694.
[47] S. Benz, U. Haeberlen and J. Tegenfeldt, J. Magn. Reson. 66 (1986) 125.
[48] H.H. Limbach, J. Hennig, R.D. Kendrick and C.S. Yannoni, J. Am. Chem. Soc. 106 (1984) 4059.
[49] H.H. Limbach, D. Gerritzen, H. Rumpel, B. Wehrle, G. Otting, H. Zimmermann, R.D. Kendrick and C.S. Yannoni, in: Photoreaktive Festkörper, eds. H. Sixl., J. Friedrich and C. Bräuchle (Wahl Verlag, Karlsruhe, 1985) S.19-43.
[50] B. Wehrle, H.H. Limbach, M. Köcher, O. Ermer and E. Vogel, Angew. Chem. 99 (1987) 914; Angew. Chem. Intern. Ed. 26 (1987) 934.
[51] H.H. Limbach, B. Wehrle, H. Zimmermann, R.D. Kendrick and C.S. Yannoni, J. Am. Chem. Soc. 109 (1987) 929.
[52] H.H. Limbach, B. Wehrle, H. Zimmermann, R.D. Kendrick and C.S. Yannoni, Angew. Chem. 99 (1987) 241; Angew. Chem. Intern. Ed. 26 (1987) 247.
[53] H.H. Limbach, B. Wehrle, M. Schlabach, R. Kendrick and C.S. Yannoni, J. Magn. Reson. 77 (1988) 84.
[54] B.H. Meier, C.B. Storm and W.L. Earl, J. Am. Chem. Soc. 108 (1986) 6072.
[55] L. Frydman, A.C. Olivieri, L.E. Diaz, B. Frydman, F.G. Morin, C.L. Mayne, D.M. Grant and A.D. Adler, J. Am. Chem. Soc. 110 (1988) 336;
L. Frydman, A.C. Olivieri, L.E. Diaz, B.A. Valasinas and B. Frydman, J. Am. Chem. Soc. 110 (1988) 5651.
[56] H.H. Limbach, T. Butenhoff and C.B. Moore, unpublished results;
T. Butenhoff and C.B. Moore, J. Am. Chem. Soc. 110 (1988) 8336.
[57] A. Sarai, J. Chem. Phys. 76 (1982) 5554; 80 (1984) 5431.
[58] G.I. Bersuker and V.Z. Polinger, Chem. Phys. 86 (1984) 57.
[59] J. Almlöf, Intern. J. Quantum Chem. 8 (1974) 915.
[60] V.A. Kutzmitsky and K.N. Solovyov, J. Mol. Struct. 65 (1980) 219.
[61] K.M. Merz and C.H. Reynolds, J. Chem. Soc. Chem. Commun. (1988) 90.
[62] Z. Smedarchina, W. Siebrand and T.A. Wildman, Chem. Phys. Letters 143 (1988) 395.
[63] C.A. Taylor, M.A. El-Bayoumi and M. Kasha, Proc. Natl. Acad. Sci. US 63 (1969) 253.
[64] I.E. Zaleskii, V.N. Kotlo, A.N. Sevchenko, K.N. Solov'ev and S.F. Shkirman, Soviet Phys. Dokl. 17 (1973) 1183.
[65] S. Völker and J.H. van der Waals, Mol. Phys. 32 (1976) 1703.
[66] S. Völker and R. Macfarlane, IBM Res. Develop. 23 (1979) 547.
[67] J.M. Clemens, R.M. Hochstrasser and H.P. Trommsdorff, J. Chem. Phys. 80 (1984) 1744.
[68] T.H. Huang, K.E. Rieckhoff and E.M. Voigt, J. Chem. Phys. 77 (1982) 3424.
[69] J. Friedrich and D. Haarer, Angew. Chem. 96 (1984) 96; Angew. Chem. Intern. Ed. 23 (1984) 113.
[70] W.E. Moerner, J. Mol. Electr. 1 (1986) 55.
[71] L.E. Webb and E.B. Fleischer, J. Chem. Phys. 43 (1965) 3100.
[72] B.M.L. Chen and A. Tulinsky, J. Am. Chem. Soc. 94 (1972) 4144.
[73] A. Tulinsky, Ann. NY Acad. Sci. 206 (1973) 47.
[74] M.J. Hamor, T.A. Hamor and J.L. Hoard, J. Am. Chem. Soc. 86 (1964) 1938.
[75] S.J. Silvers and A. Tulinsky, J. Am. Chem. Soc. 89 (1967) 3331.
[76] R.J. Butcher, G.B. Jameson and C.B. Storm, J. Am. Chem. Soc. 107 (1985) 278.
[77] M.L. Schneider, J. Chem. Soc. (1972) 1093.
[78] J.M. Robertson, J. Chem. Soc. (1935) 615 (1936) 1195.

[79] J.M. Robertson and I. Woodward, J. Chem. Soc. (1937) 219.
[80] B.F. Hoskins, S.A. Mason and J.C.B. White, J. Chem. Soc. Chem. Comm. (1969) 554.
[81] D. Berezin, Russ. J. Chem. 39 (1965) 165.
[82] F.H. Moser and A.L. Thomas, Phthalocyanine Compounds (Chapman and Hall, London, 1963).
[83] A.B.P. Lever, Advan. Inorg. Radiochem. 7 (1965) 27.
[84] M.T. Robinson and G.E. Klein, J. Am. Chem. Soc. 74 (1952) 6294.
[85] A.A. Ebert and H.B. Gottlieb, J. Am. Chem. Soc. 74 (1952) 2806.
[86] J.M. Assour, J. Phys. Chem. 69 (1965) 2295.
[87] J.H. Sharp and R.L. Miller, J. Phys. Chem. 72 (1968) 3335.
[88] M. Scalera and R.E. Brouillard, A.P. 2525621 (1946).
[89] K. Clusius and E. Effenberger, Helv. Chem. Acta 38 (1955) 1836.
[90] R.P. Linstead and A.R. Lowe, J. Chem. Soc. (1934) 1022.
[91] P.D. Ellis and F.D. Doty, Rev. Sci. Instrum. 52 (1981) 1868.
[92] W.J. Albery, P.N. Bartlett, C.P. Wilde and J.R. Darwent, J. Am. Chem. Soc. 107 (1985) 1854.
[93] G. Williams and D.C. Watts, Trans. Faraday. Soc. 66 (1970) 80.
[94] B. Wehrle and H.H. Limbach, in preparation.
[95] G.P. Moss, Pure Appl. Chem. 59 (1987) 833.